Temperature and WNK-SPAK/OSR1 Kinases Dynamically Regulate Antiviral Human GFP-MxA Biomolecular Condensates in Oral Cancer Cells

Pravin B. Sehgal *, Huijuan Yuan , Susan V. DiSenso-Browne

Posted Date: 5 March 2025

doi: 10.20944/preprints202503.0315.v1

Keywords: pathogenesis of oral cancer; anatomical sites of oral cancer; path of liquid transit through mouth; environmental hypotonic and temperature stresses; biomolecular condensates; human myxovirus resistance protein (MxA/Mx1); condensate disassembly and spontaneous reassembly; WNK-SPAK/OSR1 kinases; spheroid to fibril transitions; antiviral activity

 doi:10.20944/preprints202503.0315.v1

Article

Temperature and WNK-SPAK/OSR1 Kinases Dynamically Regulate Antiviral Human GFP-MxA Biomolecular Condensates in Oral Cancer Cells

Pravin B. Sehgal [1,2,*], Huijuan Yuan [1] and Susan V. DiSenso-Browne [3]

[1] Department of Cell Biology and Anatomy, New York Medical College, Valhalla, NY 10595, USA
[2] Department of Medicine, New York Medical College, Valhalla, NY 10595, USA
[3] Touro College of Dental Medicine at New York Medical College, Hawthorne, NY 10532, USA
* Correspondence: pravin_sehgal@nymc.edu

Abstract: Phase-separated membraneless biomolecular condensates in the cytoplasm or nucleus are now recognized to play a major role in modulating diverse functions in mammalian cells, and contribute to cancer pathogenesis. Mechanisms that regulate the partitioning of components into condensed vs dispersed phases in intact cells, and those that trigger spheroid to fibril transition of condensate structure have attracted attention. We selected a common circumstance for our investigations - all of us episodically imbibe cold and warm drinks such as water, tea, or coffee subjecting our oral epithelial cells to stresses of hypotonicity and temperature. Moreover, oral cancer, in the absence of overt causes such as tobacco or alcohol, most frequently occurs in a U-shaped zone (floor of mouth, side of tongue, anterior fauces and retromolar region) reflecting the path of liquid transit through the mouth. In previous studies, we investigated the partitioning of the broad-spectrum antiviral human MxA protein (also called Mx1) between condensate (storage granule) and dispersed (antivirally active) phases in human oral cancer cells. We had observed that at 37°C, in OECM1 oral carcinoma cells, GFP-MxA condensates were exquisitely sensitive to hypotonicity – these disassembled within 1-2 min of exposure of cells to saliva-like one-third hypotonicity, and underwent spontaneous reassembly in the next 5-7 min even when continued in hypotonic medium. In the present studies we investigated whether this process was temperature sensitive representative of cold vs warm drinks. It was slowed at 5°C, and speeded up at 50°C. The involvement in this disassembly/reassembly process of WNK-SPAK/OSR1 serine-threonine kinase pathway, which regulates water and Na, K and Cl influx and efflux, was evaluated using pathway inhibitors WNK463, WNK-IN-11 and closantel. The pan-WNK inhibitor WNK463 inhibited disassembly, while the SPAK/OSR1 inhibitor closantel markedly slowed reassembly. Unexpectedly, the WNK1-selective inhibitor (WNK-IN-11), triggered dramatic and rapid (within 1 hr) spheroid to fibril transition of GFP-MxA condensates in live cells. The latter cells retained their antiviral phenotype against vesicular stomatitis virus. Thus, overall, cellular water fluxes and temperature changes dramatically but reversibly affected the GFP-MxA condensate landscape in oral epithelial cells. The WNK-SPAK/OSR1 kinases appear to be part of a mechanism for condensate recovery and restoration. The data raise a novel condensate-dysregulation hypothesis for understanding the occurrence of oral cancer along the liquid transit pathway in the mouth.

Keywords: pathogenesis of oral cancer; anatomical sites of oral cancer; path of liquid transit through mouth; environmental hypotonic and temperature stresses; biomolecular condensates; human myxovirus resistance protein (MxA/Mx1); condensate disassembly and spontaneous reassembly; WNK-SPAK/OSR1 kinases; spheroid to fibril transitions; antiviral activity

1. Introduction

 doi:10.20944/preprints202503.0315.v1

Oral cancer, in the absence of overt causes such as tobacco or alcohol, most frequently occurs (in >95% of patients) in a U-shaped zone comprising floor of mouth, especially around the papilla of the submandibuar duct, side of tongue, anterior pillar of fauces and retromolar region which reflect the path of liquid flow through the mouth [1–3] (especially see Figures 3a and 3b in reference [2]). The lining epithelium in these regions is thin, largely non-keratinized and relatively more permeable than other regions of the mouth [2,4–7]. The cellular basis for this localization of oral cancer occurrence in this zone in the absence of any overt causes (such as in cancer of the buccal mucosa in individuals chewing tobacco or betel-nut leaves [1–3]) is incompletely understood. Possibilities investigated have included changes in the oral microbiome, including bacterial, fungal and viral agents [8–10]. The present study provides a new basis for understanding subcellular changes in oral epithelial cells along the liquid transit pathway through the mouth in terms of rapid dynamic changes in the cell biology of biomolecular condensates.

Membraneless phase-separated biomolecular condensates in the cytoplasm and the nucleus have emerged as providing scaffolding for and modulating diverse subcellular functions [11–19]. In recent years, condensate droplet formation during cellular stress responses, the regulation of translation and transcription, cancer pathogenesis through the activity of fusion oncoproteins leading to aberrant prooncogenic signaling, involvement of condensates in mechanisms of innate and adaptive immunity, cytokine signaling, viral replication and antiviral mechanisms, and the targeting of condensates by cancer therapeutic agents have been highlighted by numerous investigators [15–21]. Heterogeneous regions of structure and function within the same condensate (the nucleolus is an eminent example [1–8]) as well as diversity of function among similar condensates (inhibition vs stimulation of mRNA translation in condensate granules [22]) add to the significance of biomolecular condensates in modulation of cellular functions. Physiologically, in the intact cell, condensates show dramatic metastability through mechanisms that regulate changes in component concentrations in condensed vs dispersed phases, as well as changes in condensate size and shape (such as a spheroid to fibril transition) [13,16,17,23]. Various RNA- and DNA-containing viruses also use phase-separated structures in the cytoplasm or nucleus as locations for viral replication [17,23–31].

Five years ago, we realized that the cytoplasmic structures formed in human Huh7 hepatoma cell line by the interferon (IFN)-induced “myxoviris resistance protein” (MxA alias Mx1), a dynamin-family large GTPase (approx. 60 kDa), were membraneless biomolecular condensates of variable size and shape (but, mainly spheroidal) [17,23,32]. Human MxA is an exclusively cytoplasmic protein which has a broad-spectrum antiviral activity against various RNA- and DNA-containing viruses [33–47]. For our present purposes, MxA inhibited orthomyxoviruses such as influenza A virus and Thogota virus (these have a nuclear step in their life cycle), and the rhabdoviris vesicular stomatitis virus (VSV) (this replicates entirely in the cytoplasm) [33–39]. In cell-free assays, recombinant MxA inhibited VSV transcription, indicative of the likely targeting of “early” viral transcription by MxA in the infected cell [37,38]. Also in cell-free assays, recombinant MxA showed the ability to form oligomers, multimers and larger oligomeric structures affected by “salt” concentration in the buffers used (longer fibrils were observed at lower NaCl, 50 mM) [40]. In the cell cytoplasm, MxA formed large granular structures in IFN-treated cells or upon accumulation of exogenously expressed protein [41–45]. Mutants of MxA lacking GTPase activity, and thus lacking antiviral activity still formed granular structures in the cytoplasm [42–45]. Critically, it was recognized very early that the L612K mutant of MxA, which remained dispersed in the cytoplasm retained antiviral activity towards VSV and Thogota virus [46]. Thus, in the case of MxA, the dispersed phase (which can contain GTPase-competent dimers) was viewed as antivirally active, and the granules as a storage reservoir [46–48]. Formal quantitation of GFP-MxA in condensed vs dispersed phases, even in cell images appearing to show “almost all” GFP-MxA in condensates revealed that 10-25% of the GFP-MxA was typically in the dispersed phase likely accounting for the antiviral phenotype of such cells (see Figure 1 below) and references [17,48,49]. Clearly, mechanisms that regulate the equilibrium of MxA between condensed and dispersed phases are relevant to understanding its antiviral mechanisms.

Preprints.org (www.preprints.org) | NOT PEER-REVIEWED | Posted: 5 March 2025 doi:10.20944/preprints202503.0315.v1

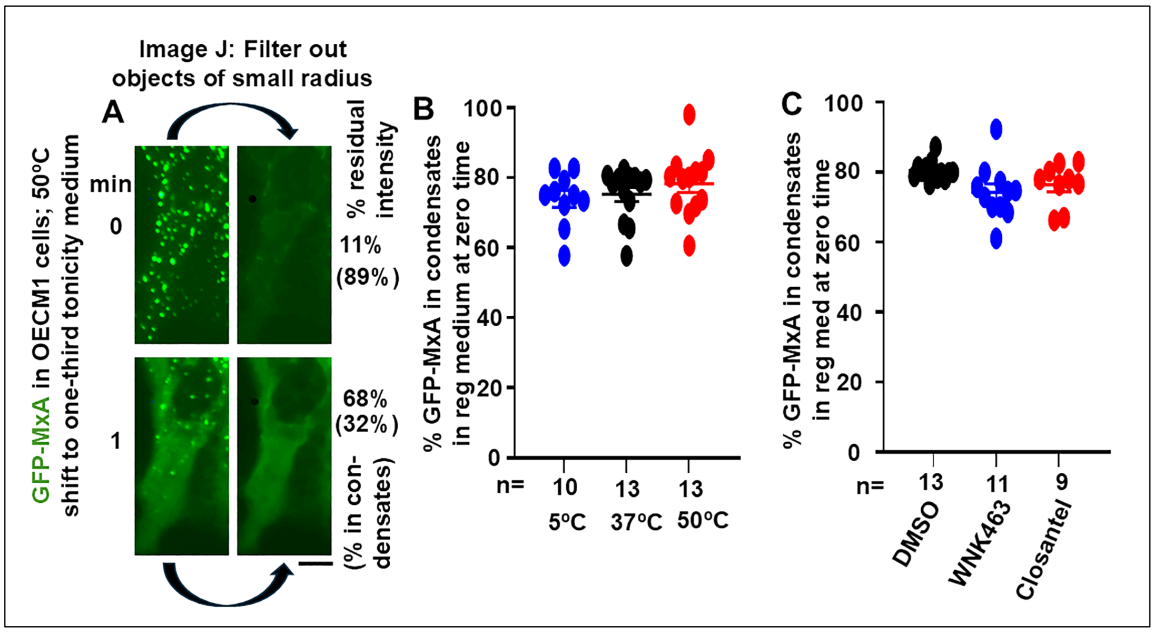

Figure 1. Quantitation of GFP-MxA in condensed vs dispersed phases. Panel A illustrates the upper left images from Figure 2A, without and with filtering out small objects of radius <4 pixels using Image J. The GFP intensities over each cell image was quantitated to give % residual intensity, and these data converted to % of GFP-MxA in condensates as indicated in parentheses. Panels B and C, multple cells (n = 9-13) at the start "zero" time in the experiments shown in Figures 3 and 4 were evaluated one hour after the appropriate exposure of cultures in isotonic culture medium. Horizonal lines are Mean ± SE. There was little significant differnce between each of the three groups in Panels B and C using ANOVA (Kruskal-Wallis) with Dunn's post-hoc test for multiple comparisons.

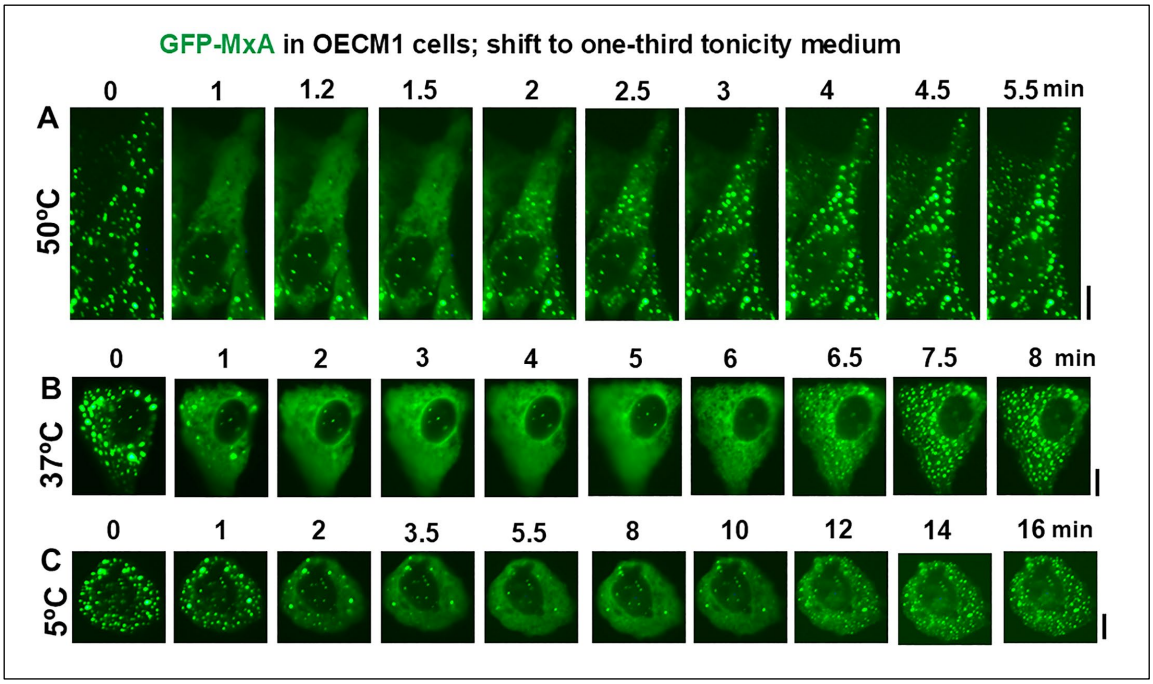

 doi:10.20944/preprints202503.0315.v1

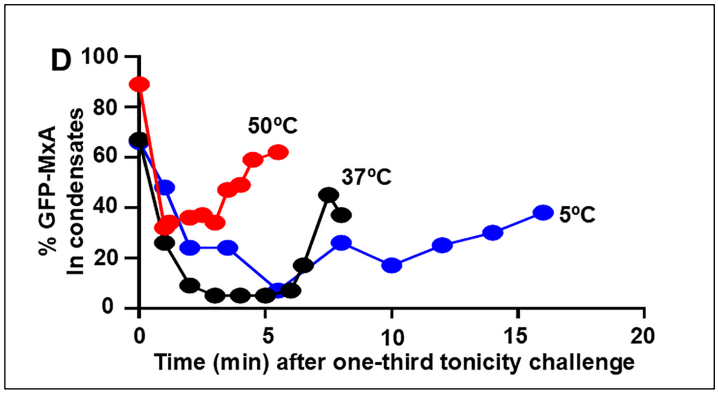

Figure 2. Panels A, B and C, OECM1 cells were either exposed to full culture medium at the indicated temperatures for approx. 60 min, and then shifted to one-third tonicity medium (corresponding to saliva-like hypotonicity; approx. 100 mOsm). Live-cell imaging was carried out as indicated. Scale bar = 10 μm. Panel D, Quantitation of % GFP-MxA per cell in condensates (in the same cells shown in Panels A, B and C).

We had already observed that cytoplasmic MxA condensates showed rapid disassembly in 1-2 min in Huh7 hepatoma cells exposed to hypotonic medium, and rapid reassembly (also in 1-2 min) in cells shifted back to isotonic medium) [23]. Mechanical pressure and oxidative stress (e.g., by placement of a coverslip on live cells, nitric oxide scavenging using c-PTIO, or exposure to dynasore) triggered a dramatic transition of GFP-MxA spheroids to motile fibrils in live cells. [23].

The hypotonicity-triggered disassembly and subsequent reassembly of GFP-MxA condensates were replicated in human A549 lung carcinoma and in human OECM1 oral squamous cell carcinoma lines [48,49]. Remarkably, in both these cancer cell lines GFP-MxA dispersed in cells exposed to moderate hypotonicity (75-100 mOsm) *spontaneously* reassembled into fresh condensates in the next 7-15 min even in cells continuously kept in the hypotonic medium, suggesting the existence of cellular mechanisms that mediated this recovery [48,49]. The focus of the present studies was to investigate the biochemical mechanisms that underlie this disassembly and spontaneous reassembly process in a biological context that would be physiologically and pathologically relevant.

For this investigation, we selected a common circumstance that applies to all of us. We all episodically imbibe cold and warm drinks such as water, tea, or coffee everyday subjecting our oral epithelial cells to stresses of hypotonicity and temperature. MxA is *constitutively* expressed in healthy human gingival epithelium, and is also induced by Type III interferons (IFNs) such as IFN-λ1 in primary gingival cells [48,50]. Moreover, fibrillar MxA structures are observed in the cytoplasm of oral epithelial cells in inflammatory lesions [51]. Typically, only IFN-λ (a Type III IFN) but not IFN-α (a Type I IFN) induce MxA in gingival epithelial cells [52]. Thus, the Type III IFNs comprising the IFN-λ species which induce MxA contribute to antiviral barrier immunity at the level of the oral cavity [48,51]. The realization that oral epithe;ial cells are constantly bathed in hypotonic saliva (normally one-third tonicity, approximately 100 mOsm, compared to plasma which is 300 mOsm) and are repeatedly exposed to environmental stresses of hypotonicity and temperature (cold and warm drinks of different tonicity = water, tea and coffee are 30-50 mOsm) led us to investigate the biochemical mechanisms that underlie GFP-MxA condensate dynamics in an oral squamous cell cancer line (OECM1) [48,52–56]. These cells in culture grew in tight epithelial sheets, and retained the original property of responding selectively to IFN-λ1 by increasing MxA granules, but not to IFN-α2 [48]. Moreover, these cells also retained the property of disassembly of GFP-MxA condensates within 1-2 min of exposure to saliva-like one-third hypotonicity (100 mOsm), and spontaneous reassembly in the next 5-7 min even when continues in saliva-like hypotonicity [48]. Additionally, GFP-MxA condensate containing cells in OECM1 cultures exposed to Lipton's tea (35 mOsm) or Colombian coffee (50 mOsm) at 37°C showed rapid condensate disassembly in 1-3 min [48]. That left open the question of the effect of temperature on this process (as in exposure to cold (5°C) or warm (50°C) drinks) and the biochemical mechanisms mediating this process as well as recovery from such stress that might function along the fluid intake channels in the mouth.

 doi:10.20944/preprints202503.0315.v1

In the present studies we used a quantitative image processing method to separate GFP-MxA in condensate objects vs dispersed phase in OECM1 cells in order to quantitatively investigate the effect of temperature on hypotonicity-triggered condensate disassembly and spontaneous reassembly process. The involvement in this process of the WNK-SPAK/OSR1 serine/threonine kinases (WNK, With-No-Lysine kinases; SPAK, STE 20/SPS1-related proline alanine-rich kinase; OSR1, oxidative stress response kinase 1) which are known to regulate aquaporins and ion transporters and co-transporters which mediate water and Na, K and Cl influx and efflux [57–62], was investigated using pharmacological tools (the pan-WNK inhibitor WNK463, the WNK1-selective inhibitor WNK-IN-11 and the SPAK/OSR1 inhibitor closantel) [61]. Unexpectedly, in these studies, we discovered that the WNK1-selective inhibitor (WNK-IN-11), triggered dramatic and rapid (within 1 hr) spheroid to fibril transition of GFP-MxA condensates in live cells. This observation allowed for a test of the antiviral phenotype against VSV of cells with fibrillar GFP-MxA vs spheroidal GFP-MxA, and more generally the relationship between different condensates of wild-type GFP-MxA and the antiviral state in single cells.

2. Materials and Methods

2.1. Cells and Cell Culture

Human oral carcinoma cell line OECM1 was purchased from Millipore-Sigma (St. Louis, MO). Human hepatoma cell line Huh7 was a gift from Dr. Charles M. Rice, The Rockefeller University (New York, NY) [23]. Human lung adenocarcinoma cell line A549 was obtained from the ATCC (Manassus, VA). Additional aliquots of the A549 cells and its derivative line A549-hACE2 were obtained from BEI Resources/ATCC (Manassus, VA). The respective cell lines were grown in DMEM (Corning Cat. No. 10-013-CV, with glutamine, Na-pyruvate and high glucose) supplemented with 10% v/v fetal bovine serum (FBS; Gibco, Grand Island, NY) in T25 flasks [23,48,49]. For experiments, the cells were typically plated in 35 mm dishes without or with cover-slip bottoms [23,48,49].

2.2. Plasmids and Transient Transfection

The GFP (1-248)-tagged full-length human MxA was a gift from Dr. Jovan Pavlovic (University of Zurich, Switzerland) [23,43]. Transient transfections were carried out using just subconfluent cultures in 35 mm plates using DNA in the range of 0.3-2 μg/culture and the Polyfect reagent (Qiagen, Germantown, MD) and the manufacturer's protocol (with 10 μl Polyfect reagent per 35 mm plate) [23,48,49].

2.3. Live-Cell Fluorescence Imaging

Live-cell imaging of GFP-MxA structures in transiently transfected cells was carried out in cells grown in 35 mm plates using the upright the Zeiss AxioImager 2 equipped with a temperature-regulated stage (range: 5-50°C) and a 40x water immersion objectivewith data capture in a manual time-lapse mode (using Axiovision 4.8.1 software) [23,48,49]. Additionaly, live-cell imaging was also carried out by placing a coverslip on the sheet of cells and imaging using a 100x oil immersion objective [23,48,49].

2.4. Phase Transition Experiments and Fluorescence Imaging

Live GFP-MxA expressing cells in 35 mm plates were imaged using a 40x water-immersion objective 1-3 days after transient transfection in growth medium at 37°C [23,48,49]. After collecting baseline images of MxA condensates at 37°C, the cultures were exposed to full growth medium for approximately 1 hr equilibrated at 5 or 37 or 49-50°C and imaged (with the stage set at the relevant temperature) (the "0 min" time). Subsequently the cultures were shifted to 1:3 or 1:6 medium (adjusted with sterile water) at the indicated temperatures, followed by time-lapse microscopy of the same filed of cells for the next 15-20 min. For inhibitor experiments, cultures were exposed to the indicated inhibitor in full medium at 37°C for approximately 50-60 min, imaged, and then shifted to

 doi:10.20944/preprints202503.0315.v1

one-fourth tonicity medium at 37C containing the same inhibitor followed by time-lapse microscopy of the same field of cells.

Fluorescence was imaged as previously reported [23,48,49] using an erect Zeiss AxioImager M2 motorized microscopy system with Zeiss W N-Achroplan 40X/NA0.75 water immersion or Zeiss EC Plan-Neofluor 100X/NA1.3 oil objectives equipped with an high-resolution RGB HRc AxioCam camera and AxioVision 4.8.1 software in a 1388 x 1040 pixel high speed color capture mode.

2.5. Quantitation of Relative Amounts of GFP-MxA in Condensates vs Dispersed State in a Cell

Briefly, cell images with mixed condensate and dispersed GFP-MxA were subjected to Filter processing to subtract ("Minimize") objects of small radii (2-4 pixels) using Image J software [17,48,49]. The pixel radius (in the range 2-5 pixels) used for the subtraction was optimized to subtract all condensates from the image. GFP-MxA intensity in the residual subtracted image corresponded to the dispersed protein; subtracting this from the total intensity per cell gave the % of MxA in condensates on a per cell basis [48,49].

2.6. VSV stock and Virus Infection

A stock of the wild-type Orsay strain of VSV (titer: 9 x 10^8 pfu/ml) was a gift from Dr. Douglas S. Lyles (Dept. of Biochemistry, Wake Forest School of Medicine, Winston-Salem, NC). Single-cycle virus infection studies at high multiplicity (moi >10 pfu/ml) were carried out essentially as described by Carey et al. [63] as summarized in Davis et al. [23]. Briefly, cultures (approx. 2 x 10^5 cells per 35 mm plate), previously transfected with the pGFP-MxA expression vector (1-2 days earlier), were replenished with 0.25 ml serum-free Eagle's medium and 10-20 µl of the concentrated VSV stock added (corresponding to MOI >10 pfu/cell). The plates were rocked every 15 min for 60 min followed by addition of 0.75 ml of full culture medium. The cultures were fixed 5-6 hr after the start of the infection using 4% PFA in isotonic PBS (1 hr at 4°C), and immunostained for VSV nucleocapsid (N) protein using an mAb provided by Dr. Douglas S. Lyles (mAb 10G4). Images were collected using the 40x water immersion objective for N-protein immunofluorescence (in red) in GFP-positive (green) and negative cells, with DAPI in blue using multicolor fluorescence imaging [23].

2.7. Antibody Reagents and Chemicals

Rabbit pAb to human MxA (H-285) (ab-95926) was purchased from Abcam Inc. (Cambridge, MA); Mouse mAb to the VSV nucleocapsid (N) designated 10G4 was a gift from Dr. Douglas S. Lyles (Wake Forest School of Medicine, NC). Respective AlexaFluor 488- and AlexaFluor 594-tagged secondary donkey antibodies to rabbit (A-11008 and A-11012) or mouse (A-21202 and A-21203) IgG were from Invitrogen Molecular Probes (Eugene, OR).

The pan-WNK kinase inhibitor WNK463 (which inhibits all four WNK1-4 enzymes) and the SPAK/OSR1 kinase inhibitor closantel were purchased from Sigma-Aldrich (St. Louis, MO), while the WNK1-selective inhibitor WNK-IN-11 was obtained from Cayman Chemical Company (Ann Arbor, MI). These were dissolved in DMSO as 10 mM stocks.

2.8. Statistical Testing

This was carried out using non-parametric ANOVA (Kruskal-Wallis) with Dunn's post-hoc test for multiple comparisons. The software used was GraphPad Prism 10.

3. Results

3.1. Quantitation of GFP-MxA in Condensed vs Dispersed Phases at the Single-Cell Level

Live-cell fluorescence imaging of transiently expressied wild-type GFP-MxA in OECM1 appears to show GFP-MxA almost exclusively in condensates (Figure 1A, upper left panel). However, this is a visual effect not sustained by formal quantitation; there is always GFP-MxA in the dispersed phase

 doi:10.20944/preprints202503.0315.v1

(Figure 1A). We carried out formal estimation of GFP-MxA in condensed vs dispersed phases at the single-cell level using subroutines in Image J (Figure 1A, and references [7,38,39]). Green fluorescence images were converted to 16-bit grayscale images, average intensity Measured over a cell outline and in a background region to provide total cell intensity. The Filter routine was used to Subtract small objects of (using "Minimum") radius in the range 2-5 pixels to delete spheroidal condensates, and the average intensity of the residual filtered image estimated (again, following background subtraction in an area of free plastic away from the cell outline). The residual intensity corresponded to GFP-MxA in the dispersed phase. This can be expressed as % of total intensity in dispersed phase, or its converse as % GFP-MxA in condensates (after subtraction from 100). Figure 1A illustrates how this was carried out using the first two upper left panels from Figure 2A. Data in Figure 1B show that in normal OECM1 cells kept at 37°C in isotonic culture medium, approximately 20-25% of GFP-MxA in cells was located in the dispersed phase (range 10-40%). Thus, even in cells whose images gave the visual appearance of an almost exclusive localization of GFP-MxA in condensates, significant GFP-MxA was present in the dispersed phase.

The data in Figure 1B also show that the partitioning of GFP-MxA between condensed vs dispersed phases was largely unaffected between cultures kept for approximately 1 hr in isotonic medium at 5, 37 or 50°C. Similarly, Figure 1C shows that this partioning was largely unaffected in cultures kept for approximately 1 hr at 37°C in isotonic medium containing the WNK-SPAK/OSR1 pathway inhibitors WNK463 (25 μM) or closantel (100 μM). The images tabulated in Figures 1A and 1B correspond to "zero-time" partition estimates of single cells (n = 9-13) from the experiments in Figures 2, 3 and 4 just before these cultures were challenged with hypotonic medium.

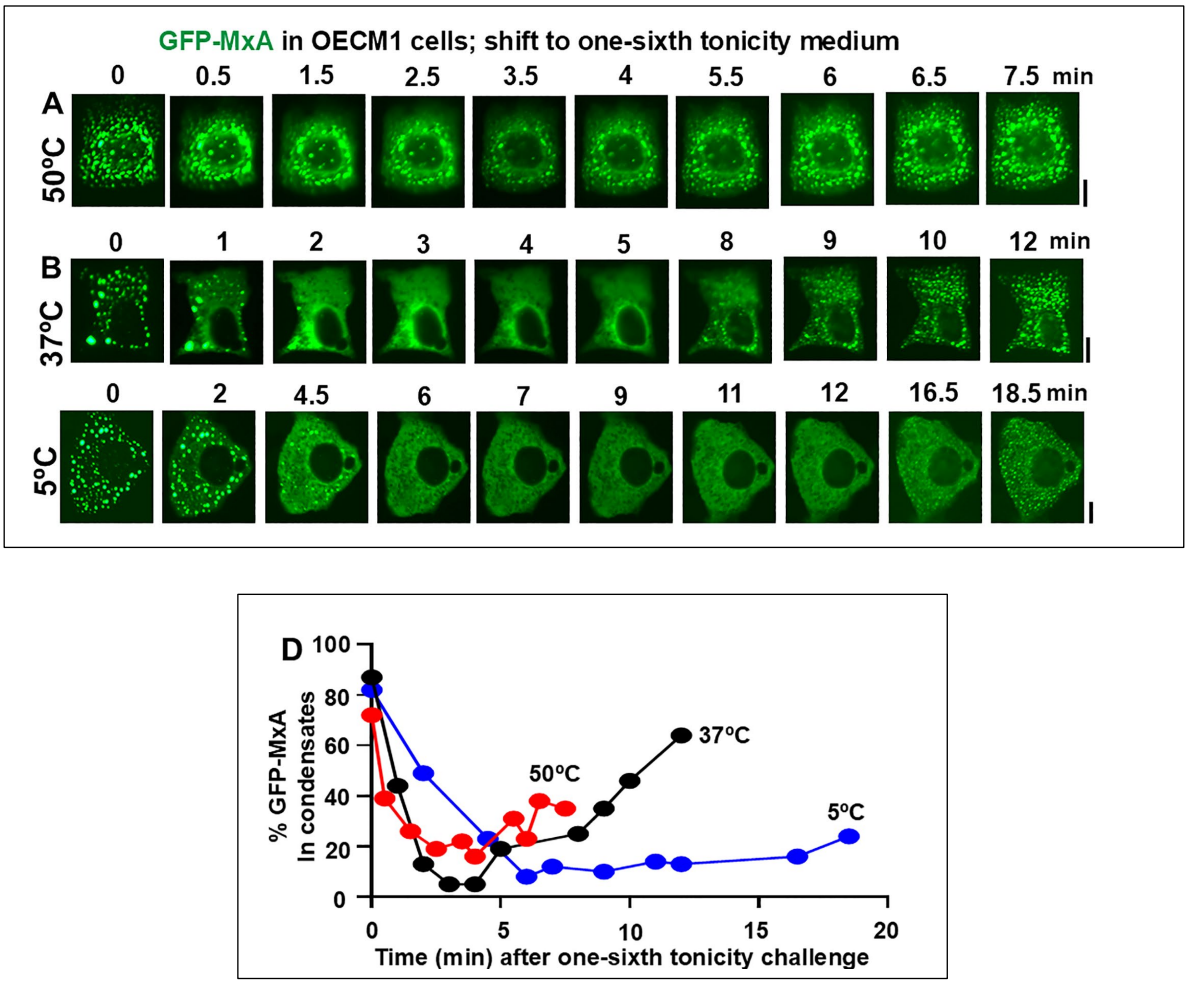

Figure 3. Panels A, B and C, OECM1 cells were exposed to full culture medium at the indicated temperatures for approx. 60 min, and then shifted to one-sixth tonicity medium (corresponding to tea- or coffee-like

 doi:10.20944/preprints202503.0315.v1

hypotonicity; approx. 50mOsm). Live-cell imaging was carried out as indicated. Scale bar = 10 μm. Panel D, Quantitation of % GFP-MxA per cell in condensates (in the same cells shown in Panels A, B and C).

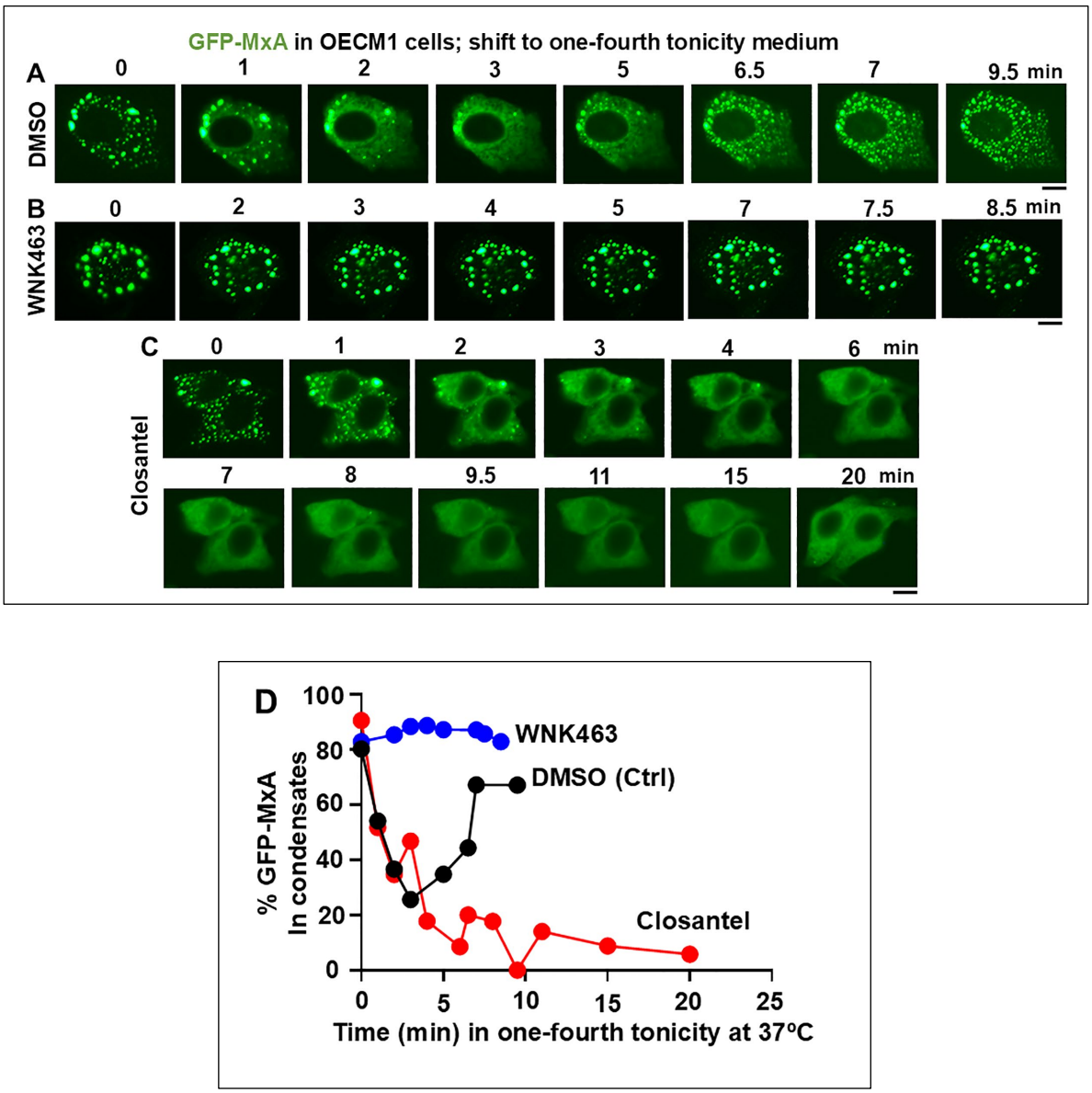

Figure 4. Panels A, B and C, OECM1 cells were either exposed to DMSO, WNK463 (25 μM) or closantel (100 μM) for at least 1 hr in full culture medium (approx. 300 mOsm), and then shifted to one-fourth tonicity medium (approx. 75 mOsm) in the continued presence of the inhibitors. Live-cell imaging was carried out as indicated. Scale bar = 10 μm. Panel D, Quantitation of % GFP-MxA per cell in condensates (in the same cells shown in Panels A, B and C).

3.2. Temperature sensitivity of the Spontaneous Reassembly of GFP-MxA Condensates Dispersed by an Hypotonic Challenge

For economy of illustration, Figures 2, 3 and 4 show detailed images and quantitation of the initial image and the subsequent full time lapse sequence of the same representative single cell for each of the experimental variables investigated. Moreover, data with respect to each of the variables illustrated in Figures 2, 3 and 4 were collected within 2-3 hours using replicate cultures plated at the same time.

The rationale for the experiment in Figure 2 was to investigate GFP-MxA condensate dynamics in oral cancer cells in cultures shifted from isotonic medium (approximately 300 mOsm) to saliva-like

 doi:10.20944/preprints202503.0315.v1

hypotonicity ("one-third tonicity" corresponding to approximately 100 mOsm). In Figure 3 the rationale was to shift oral cells from isotonic medium (300 mOsm) to beverage-like hypotonicity ("one-sixth tonicity" corresponding to approximately 50 mOsm). In each experiment, temperatures corresponding to cold (5°C) or warm (49-50°C) drinks were compared to 37°C.

Data in Figure 2B and 2D recapitulate our previous observation [48] that exposure of oral epithelial cells to one-third hypotonicity at 37°C caused a rapid disassembly of GFP-MxA condensates within 1-2 min followed by spontaneous reassembly 6-7 min later. This process was speeded up at 50°C – rapid disassembly in 1-2 min with reassembly in 2-3 min (Figure 2A and 2D). At 5°C, disassembly occurred by 2 min, but reassembly was considerably slowed to 12-16 min and remained significantly incomplete (Figure 2C and 2D). Thus, it was the reassembly process which occurs during the regulated volume decrease (RVD) part of the cell response to hypotonicity [48] that was particularly temperature sensitive.

Challenging GFP-MxA condensate-containing cells with beverage-like one-sixth hypotonicity also showed a similar temperature sensitivity (Figure 3). At 37°C, the rapid disassembly was followed by reassembly 9-12 min (Figure 3B and 3D). In comparison, reassembly was apparent by 4-5 min at 50°C (Figure 3A and 3D). However the reassembly process was slowed down to >16-18 min at 5°C (Figures 3C and 3D). Thus, again, it was the reassembly process which occurs during the regulated volume decrease (RVD) part of the cell response to hypotonicity [48] that was particularly temperature sensitive. It is noteworthy that the temperatures tested did not change the partitioning of GFP-MxA into condensed vs dispersed phases in isotonic culture medium (Figure 1B), but that the active process of reassembly during the regulated volume decrease (RVD) part of the cell response to hypotonicity was particularly temperature sensitive.

3.3. Involvement of the WNK-SPAK/OSR1 Kinase Pathway in the Dynamic Response of GFP-MxA Condensates to Hypotonicity

Our previous study of the possible biochemical mechanisms underlying GFP-MxA condensate disassembly and spontaneous reassembly following a saliva-like hypotonicity challenge suggested the involvement of protein phosphatases and their downstream target the K, Cl co-transporters (KCC; these mediate efflux of K and Cl, and thus of water) in this process [48]. Cyclosporin A which inhibits PTP2B (alias calcineurin) and tetraethylammonium chloride which inhibits KCC co-transporters slowed down the reassembly of GFP-MxA condensates [48]. In the present study we investigated involvement of known upstream components in this osmoregulatory pathway [57–62]. Exposure of cells (such as renal tubular cells) to hypotonicity activates the chloride-sensitive WNK serine-threonine kinases (WNK1-4) (reduced chloride activates the kinase) which phophorylate (and thus activate) upstream aquaporin channels as well as downstream SPAK/OSR1 kinases, which, in turn, regulate Na, K, Cl cotransporter NKCC1 (which mediates influx of these ions) and additional targets [59–62]. Thus, we investigated the effect of the pan-WNK linase inhibitor WNK463, the WNK1 kinase-selective inhibitor WNK-IN-11 and the SPAK/OSR1 kinase inhibitor closantel on the disassembly and reassembly of GFP-MxA condensates in oral cells challenged with one-fourth strength tonicity (75 mOsm) medium. In these experiments, GFP-MxA expressing OECM1 cultures were first exposed to the relevant inhibitor for approximately 60-110 min at 37°C, and imaged (as in Figure 1C). These were then challenged with one-fourth tonicity medium at 37°C containing the same inhibitor followed by time-lapse microscopy.

The data in Figure 4A and 4D confirm the disassembly of GFP-MxA in 2-3 min in cells in control culture exposed to DMSO followed by reassembly beginning in 6-7 min. In comparison, the inclusion of WNK463 inhibited/reduced the disassembly; thus, there was little scope to observe reassembly in these cells (Figure 4B and 4D). In contrast closantel allowed rapid disassembly but markedly slowed down reassembly. These data implicated the WNK-SPAK/OSR1 kinase pathway in the dynamic regulation of GFP-MxA condensates during hypotonic challenge and recovery from such a tonicity stress.

 doi:10.20944/preprints202503.0315.v1

3.4. Dramatic and Rapid Spheroid to Fibril Transition of GFP-MxA Condensates in Live Cells Triggered by the WNK1-Kinase-Selective Inhibitor WNK-IN-11

Investigation of the WNK1-selective inhibitor WNK-IN-11 (100 μM) [51] in experiments modeled on those in Figure 4, provided an unexpected observation. Live-cell imaging even before carrying out the hypotonic challenge, revealed that exposure of GFP-MxA-expressing OECM1 cultures to WNK-IN-11 showed a transition of spheroidal condensates to fibrils, Parenthetically, WNK-IN-11 had a modest effect on one-fourth tonicity triggered disassembly and slowed reassembly (data not shown). However, the more dramatic effect was a transition of GFP-MxA condensates to a fibrillar phenotype (Figure 5A). This fibrillar phenotype also developed in WNK-IN-11-treated OECM1 cultures kept continuously in isotonic medium, and also in other cancer cell lines (Figure 5B, 5C and Figure 6C). The data in Figures 5B and 5C recapitulate the spheroid to fibril transition observed observed by us previously in GFP-MxA condensates in hepatoma Huh7 cells subjected to oxidative stress (as in Figure 8 in reference [23]). Since we previously reported the association of GFP-MxA condensates with intermediate filaments in Huh7 cells [17,23], we investigated the association of GFP-MxA fibrillar condensates in Huh7 cells with intermediate filaments. As before [17,23], the data in Figure 6A and 6B show that both spheroidal and fibrillar GFP-MxA condensates in Huh7 cells were located alongside of but distinct from giantin-positive intermediate filaments. The structural transformation of GFP-MxA condensates can be rather dramatic and extensive in live A549 live lung cancer cells exposed to WNK-IN-11 for 17 hr (Figure 6E).

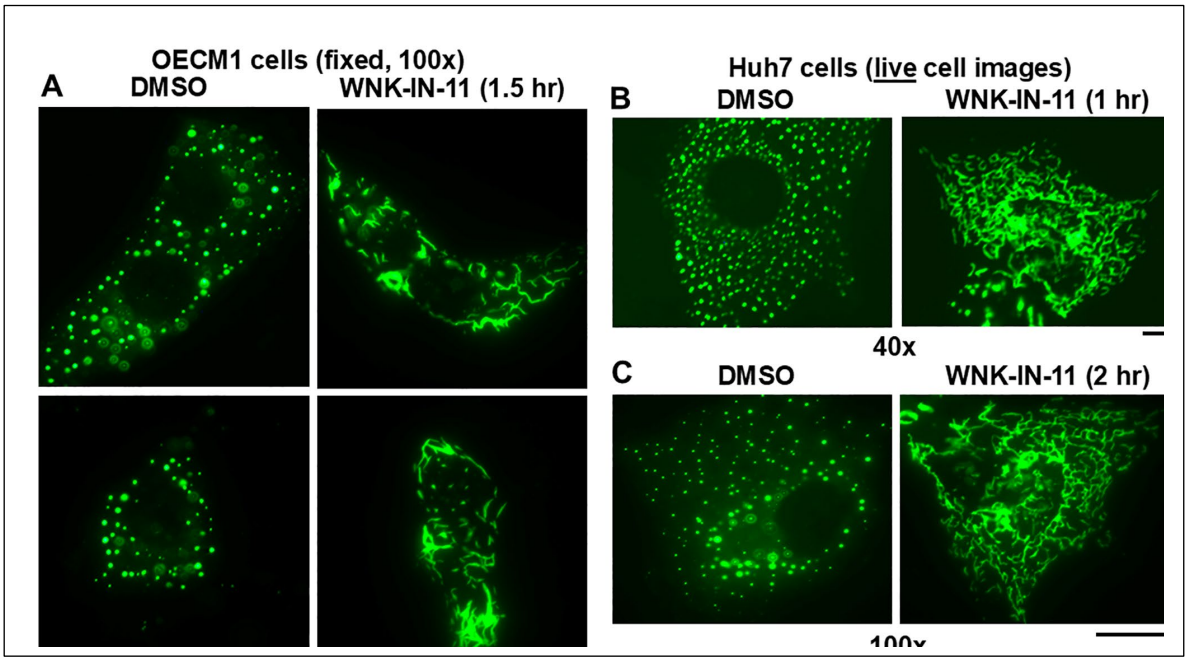

Figure 5. Spheroid to fibril transition of GFP-MxA condensates triggered by WNK-IN-11. Panels A, B and C respectively show representative OECM1 and Huh7 cells expressing GFP-MxA two days after transfection in 35 mm plates and exposed to either DMSO or WNK-IN-11 (100 μM) in isotonic regular medium at 37°C for the indicated times. Fixed and live cells were imaged using 40x or 100x objectives as indicated. Scale bars = 10 μm.

 doi:10.20944/preprints202503.0315.v1

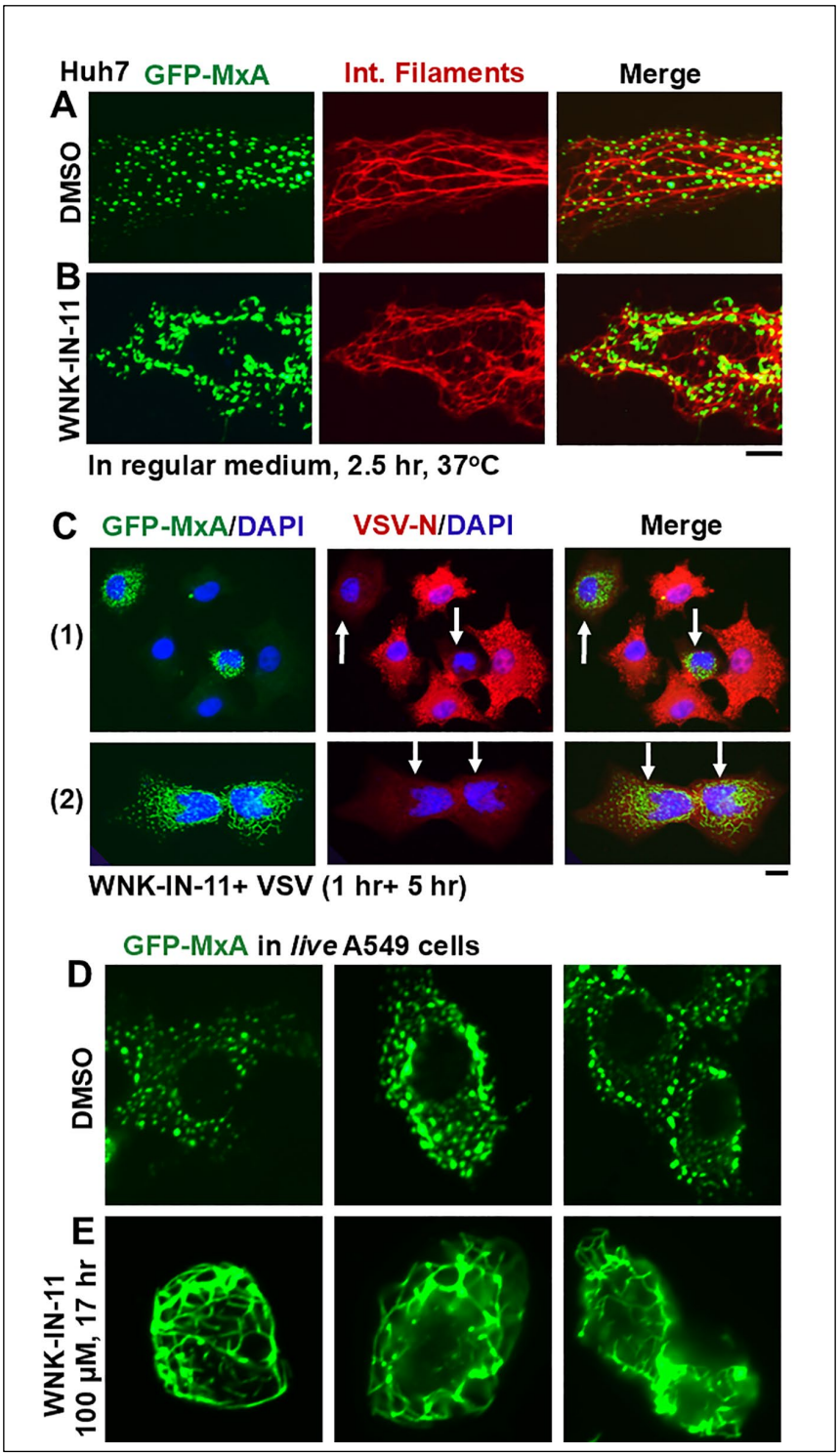

Figure 6. Properties of fibrillar GFP-MxA. Panels A and B, Huh7 cells expressing GFP-MxA were treated with DMSO or with WNK-IN-11 (100 µM) for 2.5 hr, fixed and then imaged for intermediate filaments. Panel C, A culture of Huh7 cells expressing GFP-MxA was treated with WNK-IN-11 (100 µM) for 1 hr and then exposed to VSV (moi > 10 pfu/cell) for 5 hr in the continuous presence of the inhibitor. The culture was fixed and imaged for VSV-N protein (red) in cells expressing and not expressing GFP-MxA. Sub panels (1) (showing spheroidal MxA) and (2) (showing fibrillar MxA) are from the same culture. White arrows, cells showing an antiviral phenotype. Panels D and E, Live A549 cells expressing GFP-MxA and exposed to DMSO or WNK-IN-11 (100 µM) for 17 hr were imaged as indicated. Scale bars = 100µm.

 doi:10.20944/preprints202503.0315.v1

3.5. Relationship(s) Between GFP-MxA Condensates and the Antiviral Phenotype Against VSV at the Single-Cell Level

The question of whether spheroid to fibril transition affected the antiviral activity of GFP-MxA was addressed in Huh7 cells exposed to WNK-IN-11 (100 μM) for 1 hr. While most GFP-MxA expressing cells in such cultures showed a fibrillar transition, significant numbers of cells with spheroidal condensates persisted allowing for a side-by-side comparison of the antiviral phenotype of cells of both kinds of condensates in the same culture. Such a culture was challenged with VSV at high multiplicity of infection (>10 moi/cell) and then fixed at 5-6 hr after beginning of infection followed by immunofluorescence evaluation of the accumulation of the viral nucleocapsid protein (N) [23,24]. Parenthetically, the N protein accumulates in the cytoplasm in phase-separated condensates which form centers for viral replication [24]. Figure 6C (1) and (2) show images from the same culture verifying, first, that cells with spheroidal GFP-MxA condensates showed a clear antiviral phenotype (white arrows subpanel (1)) and, second, that cells with fibrillar GFP-MxA also showed a strong antiviral phenotype (white arrows in subpanel (2)).

These studies were extended to A549 cells which had shown development of large heterogeneous GFP-MxA structures following exposure to WNK-IN-11 for 17 hr (Figure 6E). The data in Figure 7A and 7B summarize that when A549 cells were treated with WNK-IN-11 for only 1 hr prior to a VSV challenge all GFP-MxA condensate-containing cells showed a strong antiviral phenotype irrespective of the structure of the condensates. However, when cells were exposed to WNK-IN-11 overnight (17 hr) and then challenged with VSV, anomalous antiviral phenotypes became apparent. While the majority of GFP-MxA-containg cells (25/43 in this culture) showed a strong antiviral phenotype (Figure 7C shows one example; broken arrow), a subset (13/43) showed the simultaneous presence of GFP-MxA condensates together with VSV-N condenates intermixed throughout the cytoplasm (Figure 7C, white arrows). A smaller subset of cells (5/43) showed zonal areas of the cytoplasm devoid of VSV-N in the vicinity of GFP-MxA structures, with the same cells exhibiting VSV-N structures elsewhere in the cytoplasm (Figure 7D, white arrows). Thus, in these instances, the unit of antiviral phenotype was not the entire cell, but a portion of the cell, perhaps due to zonal restrictions imposed by cytoplasmic viscosity (Figure 7D). The mechanisms which regulate partitioning of GFP-MxA into the dispersed phase may regulate the apparent antiviral activity.

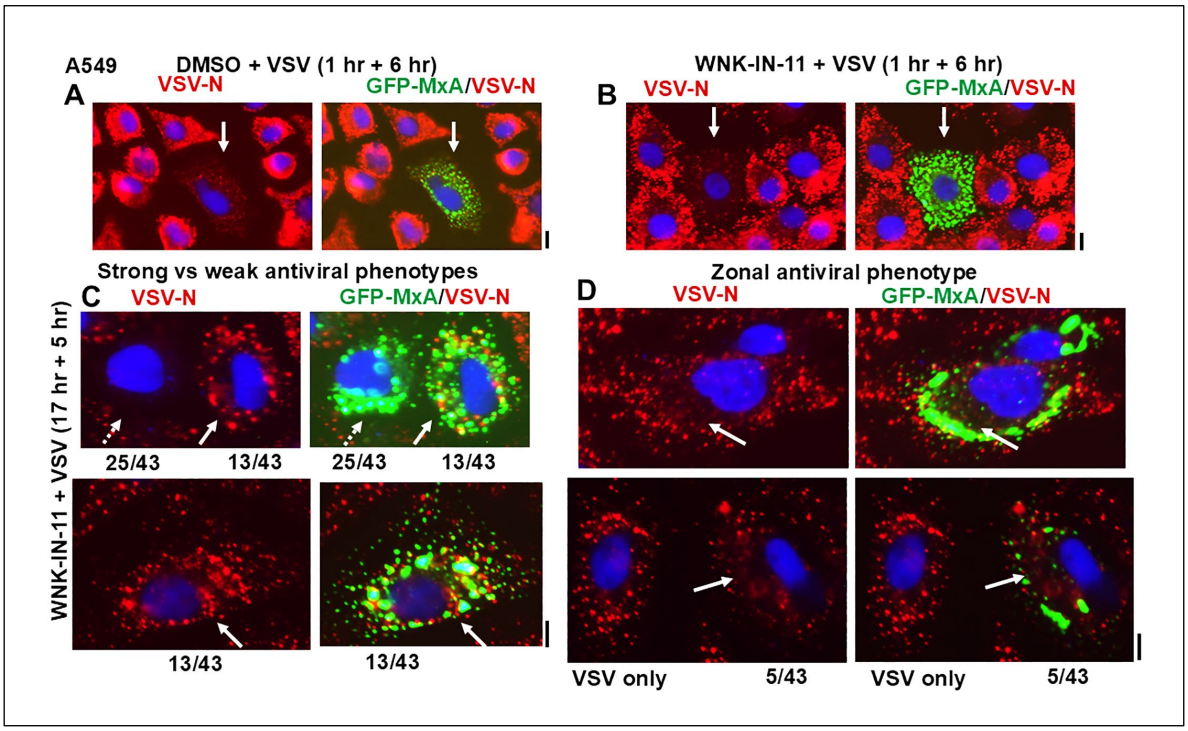

 doi:10.20944/preprints202503.0315.v1

Figure 7. Single-cell antiviral phenotypes of A549 cells containing GFP-MxA structures without or after exposure to WNK-IN-11 for 1 (Panels A and B) or 17 hr (Panel C and D) and challenged with VSV (moi > 10 pfu/cell) for 6 hr (Panels A and B) or 5 hr (Panel C). In Panels A and B, solid white arrows highlight GFP-MxA expressing cells with a strong antiviral phenotype. Panels C and D illustrative images of cells with different antiviral phenotypes out of a set of 43 GFP-positive cells scored. In Panel C, the broken arrow highlights a cell with a strong antiviral phenotype, solid white arrow highlights an adjacent and another cell with little antiviral activity. Panel D illustrates two cells with irregular GFP-MxA structures showing showing absence of virus replication in zones of the cell cytoplasm highlighted by longer solid white arrows. For comparison, Panel D (lower panels) also show a fully infected cell with no GFP-MxA. Scale bars = 10 μm.

4. Discussion

The IFN-induced human MxA/Mx1 protein forms membraneless biomolecular condensates in the cytoplasm [23,41]. While it has long been known that MxA has antiviral activity against diverse RNA- and DNA-containing viruses [33–39], the precise molecular inhibitory mechanisms against a given virus (e.g., orthomyxovirus or rhabdovirus or bunyavirus, etc) remain incompletely understood (reference [39] includes a complex summary) . While wild-type MxA forms granular structures in the cytoplasm, a mutant species of MxA (MxAL612K) which is dispersed in the cytoplasm retains antiviral activity against orthomyxovirus (Thogota virus) and rhabdovirus (VSV) [37], suggesting that partitioning of MxA between condensed and dispersed phases may regulate biological function, with MxA in the dispersed phase being the antivirally active component [46–48]. We have focused our studies on antiviral effects of human MxA against the rhabdovirus VSV because its life cycle is confined to the cytoplasm, its replication is highly sensitive to exposure of cells to all varieties of IFN, and critically, to expression of single recombinant human MxA species in the cytoplasm [23,63]. In livestock, VSV forms oral vesicular lesions, but not in immunocompetent humans [23,24,63]. In the human oral cavity, MxA is constitutively expressed in normal gingival epithelium, and is also induced by IFN-λ species (Type III IFNs) as a component mechanism of antiviral barrier immunity in the mouth [50,52]. Parenthetically, murine Mx1 is largely nuclear and, and when in this location in a cell, is largely inactive against VSV but remains active against orthomyxiviruses [33–36,64].

Oral epithelial cells (in stratified gingival or mucosal layers, or in more water-permeable locations (e.g., floor of mouth, sides of the tongue, in the gingival sulcus, in tonsillar crypts,and anterior fauces) [4–7,48,52,64] are episodically exposed to hypo- or hyper-tonicity, and different temperatures and pH from libations that we ingest. These represent a fluid transit channel in the mouth comprising the thinnest lining epithelium [2,7]. In previous studies [48] we discovered that condensates of endogenous IFN-induced human MxA as well as of exogenously-expressed GFP-MxA in oral epithelial cells were exquisitely sensitive to saliva- and beverage-like hypotonicity (range 30-100 mOsm) – exposing oral epithelial cells to hypotonicity rapidly disassembled the condensates within 1-3 min. There was then triggered an active cellular process which mediated a “spontaneous” reassembly of MxA into a different set of condensates in the next 5-10 min. This process reflected water influx and “uncrowding” of the cytoplasm in the disassembly phase, and water efflux and “recrowding” of the cytoplasm in the reassembly process – a regulated volume decrease (RVD) (Figure 8) [48].

Preprints.org (www.preprints.org) | NOT PEER-REVIEWED | Posted: 5 March 2025 doi:10.20944/preprints202503.0315.v1

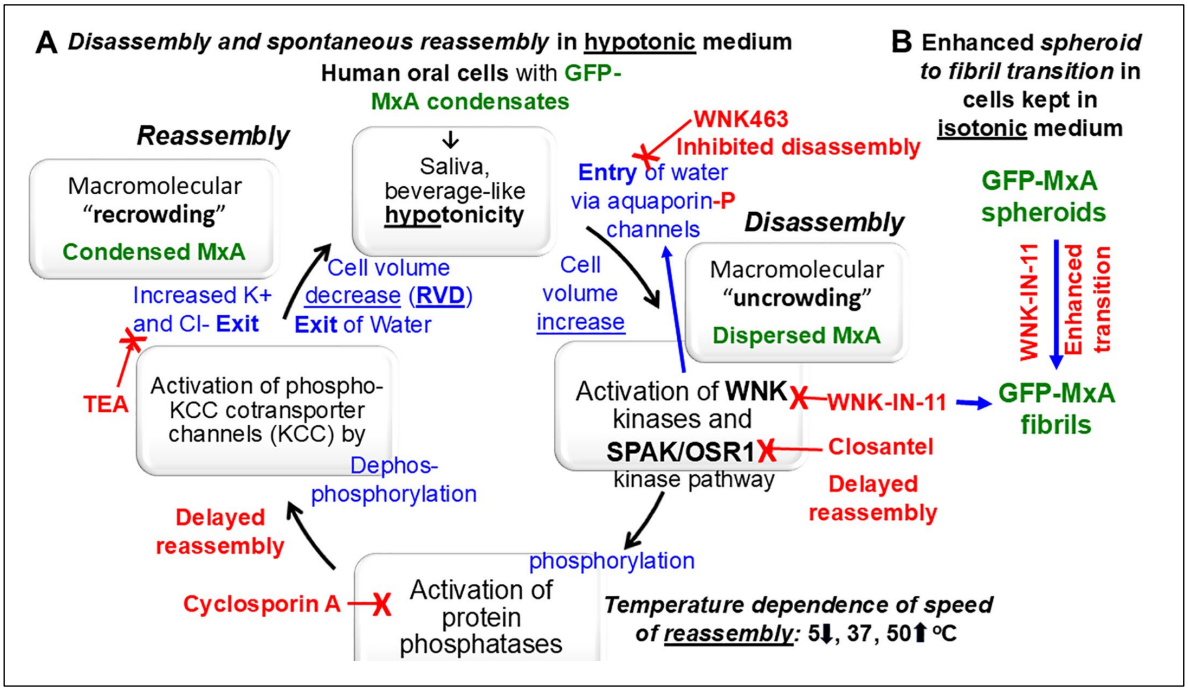

Figure 8. Schematic overview of the WNK-SPAK/OSR1 pathway involved in the dynamic disassembly and temperature-sensitive reassembly of GFP-MxA biomolecular condensates by hypotonicity (Section A), and in the spheroid to fibril transition (Section B) in oral cancer cells (adapted from Figure 9 in reference [48]).KCC, potassium-chloride cotransporter channels 1-4; OSR1, oxidative stress regulated kinase 1; SPAK, Ste-family proline and alanine enriched kinase; TEA, tetraethylammonium chloride; RVD, regulated volume decrease; WNK kinase, "With no lysine" kinase family members 1-4.

In the present studies, carried out in cultures of the OECM1 oral squamous cell carcinoma cell line (which retains the oral epithelium phenotype of MxA inducibility by IFN-λ1 but not by IFN-α2) we discovered that the reassembly of GFP-MxA condensates after hypotonicity-triggered disassembly was temperature sensitive – faster at 50ºC (corresponding to a warm drink) and slower at 5ºC (corresponding to a cold drink) (Figures 2 and 3). It was the recovery from a hypotonic challenge that was particularly temperature dependent, not so much the partitioning in regular isotonic medium (Figure 1).

The earlier discovery by us that the protein phosphatase inhibitor cyclosporin A (which inhibits PTP2B alias calcineurin) and tetraethylammonium chloride (TEA) (which inhibits K and Cl efflux through KCC co-transporters, and thus water efflux) inhibitor markedly slowed down GFP-MxA reassembly [48] suggested the involvement of the chloride-sensitive WNK kinase-SPAK/OSR1 kinase-PTP-KCC pathway in the reassembly process (Figure 8) [48].

Water and chloride are known to be allosteric inhibitors in osmosensing by WNK kinases [57–62]. Indeed, WNK1 forms tonicity-induced phase-separated biomolecular condensates (called "WNK bodies") in renal tubular cells exposed to hypertonicity [60]. In the present studies, we surmised that hypotonicity, which causes water influx through aquaporin channels, would lower cytosolic chloride concentration leading to activation of the WNK kinases and thus activation of downstream targets, eventually leading to activation of the downstream KCC2 co-transporter and consequent efflux of water and thus volume restoration (Figure 8A). This possibility was investigated in hypotonicity-driven regulation of GFP-MxA condensate disassembly and reassembly using well-characterized small-molecule inhibitors of the WNK-SPAK/OSR1 serine-threonine kinases: the pan-WNK inhibitor WNK463 which inhibits all four WNK1-4 kinases, WNK-IN-11 which is WNK1 selective, and closantel which inhibits the SPAK/OSR1 kinases [61]. As background, phosphorylation of aquaporin channel proteins by WNK kinases contributes to their water-flux activity (Figure 8) [61]. Exposing OECM1 cells to the pan-WNK kinase inhibitor WNK463 for 1 hr reduced the ability of hypotonicity

 doi:10.20944/preprints202503.0315.v1

to disassemble GFP-MxA, consistent with a reduction of water influx through aquaporin channels (Figure 4A and 4D). In contrast, closantel, an inhibitor of the downstream SPAK/OSR1 serine-threonine kinases did not affect disassembly but markedly slowed down the reassembly process (Figure 4C and 4D).

WNK1 is known to phosphorylate, and thus maintain or enhance the activity of the NKCC1 cotransporter which mediates influx of Na, K and Cl into cells [65,66]. The WNK1-selective inhibitor WNK-IN-11, had only modest effects on the disassembly-reassembly process (it inhibits only one of the four WNK kinases) but caused a dramatic and rapid (within 1 hr) spheroid to fibril transition of GFP-MxA condensates in three different cancer cell lines (Figures 5A, 5B and 6D, Figure 8B). This spheroid to fibril transition was triggered even in cells kept in isotonic medium (Figure 5, Figure 8B). The new observations showing WNK-IN-11-triggered GFP-MxA fibril formation in Huh7 cells (Fiure 5B, 5C) are similar to our previous findings of the formation of fibrillar GFP-MxA networks in live Huh7 cells subjected to oxidative stress [23]. Additionally, and in confirmation of previous observations in Huh7 cells [23], spheroidal and fibrillar GFP-MxA condensates were located alongside but were distinct from giantin-containing intermediate filaments (Figure 6A and 6B). The overnight (17 hr) exposure of A549 cells produced accumulation of GFP-MxA in larger, even vacuolar, condensates (Figure 6D).

Of relevance here is that Kochs et al. reported in 2002 [40] that in cell-free studies recombinant MxA self-assembled into long fibrils under "low salt" conditions. In their cell-free assays, "low" NaCl referred to 50 mM [40]. For comparison, in live cell cytosol Na concentration is at approximately 10-15 mEq [68]; it is possible that the known inhibition of NKCC1 cotransporter activity by WNK-IN-11 [61,67] may "lower" cytosolic Na, triggering a fibrillar transition of GFP-MxA condensates comparable to that reported in Figure 1 in reference [40]. More recently, the data of Imanulli et al. showed that human MxA in the cytoplasm of oral epithelial cells in mucosal lesions of graft versus host reaction (GVHD) were fibrillar in structure [50].

Biologically, to a first approximation, cells with fibrillar or larger mesoscale GFP-MxA structures of any shape retained a strong antiviral phenotype towards VSV (Figure 6C and 7A, 7B). However, the anomalous antiviral phenotypes illustrated in Figure 7C suggest involvement of cellular functions in regulating the antiviral activity of GFP-MxA – not all WNK-IN-11-treated A549 cells containing GFP-MxA condensates exhibited an antiviral phenotype (Figure 6C). The underlying biochemistry is likely to involve as yet unknown effects of this kinase inhibitor on the partitioning of GFP-MxA between the condensed (storage) and dispersed (antivirally active) phases.

The cytoplasm is not the only cellular compartment in which condensates show hypotonicity-driven disassembly and subsequent reassembly. Nuclear condensates of murine GFP-Mx1 formed by exogenously expressed wild-type protein either in human or murine cells [64], and IL-6-induced cytoplasmic and nuclear STAT3 condensates in hepatoma cells [68,69] also disassembled when cultures were exposed to hypotonicity (40-50 mOsm) and rapidly reassembled when cells were shifted to isotonic medium. It is likely that hypotonicity-driven uncrowding and subsequent recrowding of cellular compartments [48] are likely to broadly regulate the condensate landscape of both cytoplasmic and nuclear compartments in of oral epithelial cells.

WNK kinases and the downstream SPAK/OSR1 kinases are implicated in the migration, proliferation and metastasis of human gliomas, hepatocellular corcinoma, breast cancer and colon cancer *[61,70–72]*. In the activation of the WNK pathway in gliomas, there is direct relationship between cell volume preservation by the WNK-SPAK/OSR1 pathway components and tumor aggressiveness [70,72]. It is also now known that this pathway activates several downstream signaling cascades such as Akt, MAPK, TGF-β. GSK3β and Wnt signaling involved in cancer progression [61]. However, none of the studies thus far have considered alterations of relevant signaling through changes in biomolecular condensates mediated by aberrant activation of the WNK-SPAK/OSR1 cascade in cancer cells.

Remarkably, the sites of occurrence of oral cancer (in patients without other overt causes such as tobacco or alcohol use) follow a U-shaped distribution along the floor of the mouth, sides of the

 doi:10.20944/preprints202503.0315.v1

tongue, and the anterior fauces and retromolar region [1,2]. This represents the liquid transit channel through the mouth and here the oral mucosa is the thinnest and is the most permeable *[4–7]*. We suggest that the constant and repetitive disassembly and reassembly of diverse cytoplasmic and nuclear condensates (thus, of not only just MxA condenates) in cells along this track due to stresses of hypotonicity and temperature may contribute to the process of cancer pathogenesis in these locations. Aberrations of cellular signaling by fusion oncoproteins which trigger cancer pathogenesis through abnormal condensate formation is now well established (reviewed in [18,19]).

A limitation of the present studies is that the human OECM1 oral squamous cancer cell line was used as a representative of the oral epithelium. Although OECM1 cells retain key properties of the oral epthelium (grow in tight sheets, and MxA is induced in these cells by IFN-λ1, a Type III interferon, but not by IFN-α2, a Type I interferon [48]), a next step would be to include additional oral cancer cell lines and to also evaluate primary human gingival or immortalized gingival cell lines in these investigations.

5. Conclusions

All of us repeatedly challenge our oral mucosa with the stresses of tonicity and temperature every single day. The stratification and keratinazation of the lining epithelium is an important mechanical defense. However, water permeable regions of the oral mucosa (e.g., floor of the mouth, sides of the tongue, in the giningival sulcus, the anterior fauces and tonsillar crypts) [*4–7,52,73*] expose the underlying cells to environmental stress. Working with an oral squamous carcinoma cells line we discovered that oral epithelial cells possessed a biochemical defense mechansim comprising of the WNK-SPAK/OSR1 kinase pathway triggered by hypotonicity which ensured rapid cell volume recovery of the cells. In studies in live cells, this pathway mediated rapid and dynamic changes in the partitioning of the antiviral human GFP-MxA protein between condensed storage granules and the dispersed state. The recovery phase of these GFP-MxA biomolecular condensates was particularly sensitive to cold (5^{o}C) and warm (50^{o}C) temperatures (slowed down or speeded up respectively). The present data raise the novel possibility that cold and warm hypotonic drinks (water, tea or coffee) may broadly alter the cytoplasmic and nuclear condensate landscape in oral epithelial cells, and thus alter barrier immunity functions of the oral mucosa. Importantly, the data suggest a novel subcellular mechanism to consider in understanding the known preferential occurrence of oral cancer along the fluid transit pathway in the mouth [2]. The data also reinforce that oral hygiene should include gargling with warm salt water for fastest recovery of the condensate landscape in the oral mucosa.

Author Contributions: PBS designed the study, PBS, carried out most of the experiments and imaging, HY carried out all the plasmid DNA preparations, and SdiS-B collected imaging data in the temperature-dependence experiments. PBS and HY carried out the image quantitation and analyses, PBS wrote the manuscript. All authors approved the manuscript.

Funding: This research was supported by a grant from the New York Medical College, and personal funds of PBS.

Acknowledgments: We thank Jovan Pavlovic (University of Zurich) for the gift of the pGFP-MxA (human) expression vector [23], and Douglas S. Lyles (Wake Forest School of Medicine) for the gift of VSV virus stock. We also thank Joseph D. Etlinger (New York Medical College), Kenneth M. Lerea (New York Medical College), and Eliana Scemes (New York Medical College) numerous helpful discussions.

Data availability statement: All data are available within the manuscript.

Conflict of interest: All authors declare the absence of any conflict of interest. New York Medical College had no role in the design of the study; in the collection, analyses, or interpretation of data; in the writing of the manuscript, or in the decision to publish the results.

References

 doi:10.20944/preprints202503.0315.v1

1. Cawson, R.A. Premalignant lesions in the mouth. *Br Med Bull* **1975,** *31,* 164-170.
2. Mashberg, A., Meyers, H. Anatomical site and size of 222 early asymptomatic oral squamous cell carcinomas. *Cancer* **1976**, *37,* 2149-2157.
3. Rivera, C. Essentials of oral cancer. *Int J Clin Exp Pathol* **2015**, *8,* 11884-11894.
4. Squier, C.A. The permeability of keratinized and non-keratinized oral epithelium to horse radish peroxidase. *J Ultrastruct Res* **1973,** *43,* 160-177.
5. Squier, C.A., Rooney, L. The permeability of keratinized and nonkeratinized oral epithelium to lanthanum in vivo. *J Ultrastruct Res* **1976,** 286-295.
6. Squier, C.A., Hall, B.K. The permeability of skin and oral mucosa to water and horseradish peroxidase as related to the thickness of permeability barrier. *J Invest Dermatol* **1985,** *84,* 176-179.
7. Lesch, C.A., Squier, C.A., Cruchley, A., Williams, D.M., Speight, P. The permeability of human oral mucosa and skin to water. *J Dent Res* **1989,** *68,* 1345-1349.
8. Gholizadeh, P., Eslami, H., Yousefi, M., Asgharzadeh, M., Aghazadeh, M., Kafil, H.S. Role of oral microbiome on oral cancers: a review. *Biomed Pharmacotherapy* **2016,** *84,* 552-558.
9. Galvin, S., Moran, G.P., Healy, C.M. Influence of site and smoking on malignant transformation in the oral cavity: is microbiome the missing link? *Front Oral Health* **2023**, *4,* 1166037.
10. Lim, Y.X., D'Silva, N.J. HPV-associated oropharyngeal cancer: in search of surrogate biomarkers for early lesions. *Oncogene* **2024,** *43,* 543-554.
11. Mitrea, D.M.; Kriwacki, R.W. Phase separation in biology, functional organization of a higher order. *Cell Commun. Signal* **2016,** *14*, 1. doi:10.1186/s12964-015- 0125-7.
12. Banani, S.F., Lee, H.O., Hyman, A.A. and Rosen, M.K. Biomolecular condensates: organizers of cellular biochemistry. *Nat Rev Mol Cell Biol.* **2017,** *18***,** 285-298.
13. Shin, Y. and Brangwynne, C.P. Liquid phase condensation in cell physiology and disease. *Science* **2017,** *357(6357*) pii: eaaf4382. doi: 10.1126/science.aaf4382.
14. Alberti, S. The wisdom of crowds: regulating cell function through condensed states of living matter. *J Cell Sci.* **2017,** *130***,** 2789-2796.
15. Gomes, E.; Shorter. J. The molecular language of membraneless organelles. *J Biol Chem* **2019,** *294,* 7115-7127.
16. Alberti, S., Gladfelter, A. and Mittag, T. Considerations and challenges in studying liquid-liquid phase separation and biomolecular condensates. Cell **2019,** *176***,** 419-434.
17. Sehgal, P. B., Westley, J., Lerea, K. M. DiSenso-Browne, S. and Etlinger, J. D. (2020) Biomolecular condensates in cell biology and virology: phase-separated membraneless organelles (MLOs). *Analytical Biochem* **2020**, *597,* 113691.
18. Jiang, L., Kang, Y. Biomolecular condensates: a new lens on cancer biology. *BBA Reviews on Cancer* **1880,** 189245
19. Boija, A., Klein, I.A., Young, R.A. Biomolecular condensates and cancer. *Cancer Cell* **2021,** *39***,** 174-192**.**
20. Han, T.W., Portz, B., Young, R.A., Boija, A., Klein, I.A. RNA and condensates: disease implications and therapeutic opportunities. *Cell Chem Biol* **2020,** *31,* 1593-1609.
21. Tripathi, S., Shimekhi, H.K., Gorman, S.D., Chandra, B., Baggett, D.W. et al. Defining the condensate landscape of fusion oncoproteins. *Nat Commun* **2023,** *14,* 6008.
22. Chen, R., Stainier, W., Dufourt, J., Lagha, M., Lehmann, R. Direct observation of translational activation by a ribionucleoprotein granule. *Nat Cell Biol* **2024,** *26*, 1322-1335.
23. Davis, D., Yuan, H., Liang, F.X., Yang, Y.M., Westley, J., Petzold, C., Dancel-Manning, K., Deng, Y., Sall, J. and Sehgal, P.B. Human antiviral protein MxA forms novel metastable membraneless cytoplasmic condensates exhibiting rapid reversible tonicity- driven phase transitions. *J Virol.* **2019,** *93,* e01014-19.
24. Heinrich, B.S., Maliga, Z., Stein, D.A., Hyman, A.A. and Whelan, S.P.J. Phase transitions drive the formation of vesicular stomatitis virus replication compartments. *MBio* **2018,** *9,* e02290-17. doi: 10.1128/mBio.02290-17.
25. Dinh, P.X., Beurs, L.K., Das, P.B., Panda, D., Das, A. and Pattnaik, A.K. Induction of stress granule-like structures in vesicular stomatitis virus-infected cells. *J Virol* **2013,** *87***,** 372-383.

 doi:10.20944/preprints202503.0315.v1

26. Nikolic, J., Bars, R.L., Lama, Z., Scrima, N., Lagaudriere-Gesbet, C., Gaudin, Y. and Blondel, D. Negri bodies are viral factories with properties of liquid organelles. *Nat Commun* **2017,** *8,* 58. doi:10.1038/s41467-017-00102-9.
27. Hoenen, T., Shabman, R.S., Groseth, A., Herwig, A., Weber, M., Schudt, G., Dolnik, O., Basler, C.F., Becker, S. and Feldmann, H. Inclusion bodies are a site of ebolavirus replication. *J. Virol* **2012,** *86,* 11779-11788.
28. Alenquer, M., Vale-Costa, S., Sousa, A.L., Etibor, T.A., Ferreira, F. and Amorim. M.J. Influenza A virus ribonucleoproteins form liquid organelles at endoplasmic reticulum exit sites. *Nature Comm* **2019,** *10***,** 1629. https://doi.org/10.1038/s41467-019-09549- 4.
29. Peng, Q., Wang, L., Qin, Z., Wang, J., Zheng X., Wei, L., Zhang, X., Zhang, X. Liu, C., Li, Z., Wu, Y., Li, G., Yan, Q., Ma, J. Phase separation of Epstein-Barr virus EBNA2 and its coactivator EBNALP controls gene expression. *J. Virol.* **2020,** DOI: 10.1128/JVI.01771-19
30. Cubuk, J., Alston, J. J., Incicco, J. J., Singh, S., Stuchell-Brereton, M. D., Ward, M. D., Zimmerman, M. I., Vithani, N., Griffith, D., Wagoner, J. A., Bowman, G. R., Hall, K. B., Soranno, A. and Holehouse, A. S. The SARS-CoV-2 nucleocapsid protein is dynamic, disordered, and phase separates with RNA, *Nature Commun* **2021**, *12***,** 1936
31. Perdikari, T. M., Murthy, A. C., Ryan, V. H., Watters, S., Naik, M. T. and Fawzi, N. L. SARSCoV-2 nucleocapsid protein undergoes liquid-liquid phase separation stimulated by RNA and partitions into phases of human ribonucleoproteins, *EMBO J* **2020**, *39*, e106478
32. Davis, D.; Yuan, H.; Yang, Y.M.; Liang, F.X.; Sehgal. P.B. Interferon-alpha- induced cytoplasmic MxA structures in hepatoma Huh7 and primary endothelial cells. *Contemp Oncol (Pozn)* **2018,** *22,* 86-94.
33. Haller, O. and Kochs, G. Interferon-induced mx proteins: dynamin-like GTPases with antiviral activity. *Traffic* ***2002,*** *3,* 710-717.
34. Haller, O., Staeheli, P., Kochs, G. Interferon-induced Mx proteins in antiviral host defense. *Biochimie* ***2007,*** *89,* 812-818.
35. Haller, O., Staeheli, P., Schwemmle, M. and Kochs, G. Mx GTPases: dynamin- like antiviral machines of innate immunity. *Trends Microbiol* **215,** *23,* **1**54-163.
36. Verhelst, J., Hulpiau, P. and Saelens, X. Mx proteins: antiviral gatekeepers that restrain the uninvited. *Microbiol. Mol. Biol. Rev.* **213,** *77***,** 551-566.
37. Staeheli, P., Pavlovic, J. Inhibition of vesicular stomatitis virus mRNA synthesis by human MxA protein. *J Virol* **1991,** *65***,** 4498-4501.
38. Schwemmle, M.,Weining, K.C., Richter, M.F., Shumacher B., Staeheli, P. Vesicular stomatitis virus transcription inhibited by purified MxA protein. *Virology* **1996**, *206,* 545-554.
39. Steiner, F., Pavlovic, J. Subcellular localization of MxB determines its antiviral potential against influenza virus. *J Virol* ***2020,*** *94***,** e00125-e220
40. Kochs, G.; Haener, M.; Aebi, U.; Haller, O. Self-assembly of human MxA GTPase into highly ordered dynamin-like oligomers. *J Biol Chem* **2002,** *277*, 14172-14176.
41. Kochs, G.; Janzen, C.; Hohenberg, H.; Haller, O. Antivirally active MxA protein sequesters La Crosse virus nucleocapsid protein into perinuclear complexes. *Proc Natl Acad Sci USA* **2002,** *99,* 3153-3158.
42. Haller, O.; Gao, S.; von der Malsburg, A.; Daumke, O.; Kochs, G. Dynamin-like MxA GTPase: structural insights into oligomerization and implications for antiviral activity. *J Biol Chem* **2010,** *285*, 28419-28424.
43. Nigg, P. E.; Pavlovic, J. Oligomerization and GTP-binding requirements of MxA for viral target recognition and antiviral activity against influenza A virus. *J Biol Chem* **2015,** *290*, 29893-29906.
44. Dick, A.; Graf, L.; Olal, D.; von der Malsburg, A.; Gao, S.; Kochs, G.; Daumke, O. Role of nucleotide binding and GTPase domain dimerization in dynamin-like myxovirus resistance protein A for GTPase activation and antiviral activity. *J Biol Chem* **2015, *290***, 12779-12792.
45. Graf, L.; Dick, A.; Sendker, F.; Barth, E.; Marz, M.; Daumke, O.; Kochs, G. Effects of allelic variations in the human myxovirus resistance protein A on its antiviral activity. *J Biol Chem* **2018,** *293*, 3056-3072.
46. Janzen, C., Kochs, G., Haller, O. A monomeric GTPase-negative MxA mutant with antiviral activity. *J Virol* **2000,** *74,* 8202-8206.
47. DiPaolo, C., Hefti, H. P., Meli, M., Landis, H., and Pavlovic, J. Intramolecular backfolding of the carboxyl-terminal end of MxA protein is a prerequisite for its oligomerization. *J Biol Chem* **1999,** *274***,** 32071-32078.

 doi:10.20944/preprints202503.0315.v1

48. Sehgal, P.B., Yuan, H., Centone, A., DiSenso-Browne, S.V. Oral antiviral defesnse: saliva- and beverage-like hypotonicity dynamically regulate formation of membraneless biomolecular condensates of antiviral human MxA in oral epithelial cells. *Cells* **2024,** *13,* 590.
49. Sehgal, P.B., Yuan, H., Jin, Y. Rapid reversible osmoregulation of cytoplasmic biomolecular condensates of human interferon-α-induced antiviral MxA GTPase. *Intl J Mol Sci* **2022,** *23,* 12739.
50. Mahanonda, R., Sa-Ard-Iam, N., Rerkyen, P., et al. (2012) MxA expression induced by α-defensin in healthy human periodontal tissue. *Eur J Immunol* **2012,** *42,* 946-956.
51. Imangulli, M.M., Swaim, W.D., League, S. C., Gress, R.E., Pavletic, S. Z. Hakim, F. T. Increased T-bet+ cytotoxic effectors and type I interferon-mediated processes in chronic graft-versus-host disease of the oral mucosa. *Blood* **2009,** *113*, 3620-3630.
52. Rodriquez-Hernandez, C.J., Sokolski, K.J., Stocke, K.S. et al. Microbiome-mediated incapacitation of interferon lambda production in the oral mucosa. *Proc Natl Acad Sci USA* **2021,** *118*, e2105170118.
53. Santos, M.T.B.R., Ferreira, M.C.D., Guare, R.O. et al. Gingivitis and salivary osmolality in children with cerebral palsy. *Int J Paediatr Dent* **2016,** *26,* 463-470.
54. Ruiz, L.A., Diniz, M.B, Loyola-Rodriguez, J.P., et al. A controlled study comparing salivary osmolality, caries experience and caries risk in patients with cerebral palsy. *Med Oral Patol Oral Cir Bucal* **2018,** *23*, e211-5.
55. Feldman, M, Barnett, C. Relationships between the acidity and osmolality of popular beverages and reported postprandial heartburn. *Gasteroenterology* **1995,** *108,* 125-131.
56. Gresz, V., Kwon, T. H., Hurley, P. T., Varga, G., Zelles, T., Nielsen, S., Case, R. M., Steward, M. C. Identification and localization of aquaporin water channels in human salivary glands. *Am J Physiol Gastroint Liver Physiol* **2001,** *281:* G247-G254.
57. Shen, M.R., Chou, C.Y., Ellory, J.C. Volume-sensitive KCl cotransport associated with human cervical carcinogenesis. *Pflugers Archiv* ***2000,*** *440*, 751-760.
58. Bize, I., Guvenc, B., Robb, A., Buchbinder, G., Brugnara, C. Serine/threonine protein phosphatases a2d regulation of K-Cl cotransport in human erythrocytes. *Am J Physiol* **1999**, 277, C926-C936.
59. Akella, R., Humphreys J. M., Sekulski K., He, H., Durbacz, M. et al. Osmosensing by WNK kinases. *Mol Biol Cell* **2021,** *32* **;** 1614-1623.
60. Boyd-Shiwarski, C. R., Shiwarski, D. J., Griffths S. E., Beacham, R. T., Norrell, L. et al. WNK kinases sense molecular crowding and rescue cell volume via phase separation. *Cell* **2022,** *185,* 4488-4506.
61. Xiu, M., Li, Y., Gao, Y. An update regarding the role of WNK kinases in cancer. *Cell Death and Disease* **2022,** *13,* 795.
62. Teixeira, L.R., Akella, R., Humphreys, J.M., He, H., Goldsmith, E.J. Water and chloride as allosteric inhibitors in WNK kinase osmosensing. *eLife* **2024,** *12, RP88224.*
63. Carey, B. L, Ahmed, M., Puckett, S., Lyles, D. S. Early steps of the virus replication cycle are inhibited in prostate cancer cells resistant to oncolytic vesicular stomatitis virus. *J Virol* **2008,** ***82****:*12104-12115.
64. Sehgal, P. B., Yuan, H., Scott, M. F., Deng, Y., Liang, F-X. and Mackiewicz, A. Murine GFP-Mx1 forms phase-separated nuclear condensates and associates with cytoplasmic intermediate filaments: novel antiviral activity against vesicular stomatitis virus. *J Biol Chem* **2020,** *294,* 15218-15234
65. Thomson, MN, Cuevas, C.A., Bewarder, T.M., Dittmayer, C., Miller, L.N. et al. WNK bodies cluster WNK4 and SPAK/OSR1 to promote NCC activation in hypokalemia. *Am J Physiol Renal Physion* **318,** F216-F228.
66. 66 Zhu, W., Begum, G., Pointer, K., Clark, P.A., Yang, S.S., Lin, S.H., Kahle, K.T., Kuo, J.S., Sun, D. WMK1-OSR1 kinase-mediated phospho-activation of Na^+-K^+-$2Cl^-$ cotransporter facilitates glioma migration. *Molecular Cancer* **2014,** *13,* 31.
67. Lewis, JL, III. Water and sodium balance. *Merck Manual Professional Version*, **2024,** Merck & Co., Inc, Rahway, NJ, USA
68. Sehgal, P.B. Biomolecular condensates in cancer cell biology: interleukin-6-induced cytoplasmic and nuclear STAT3/PY-STAT3 condensates in hepatoma cells. *Contemp Oncol (Pozn)* **2019,** *23,* 16-22.
69. Sehgal, P.B. Interleukin-6 at the host-tumor interface: STAT3 in biomolecular condensates in cancer cells. *Cells* **2022,** *11,* 1164.

 doi:10.20944/preprints202503.0315.v1

70. Haas, B.R., Cuddapah, V.A., Watkins, S., Rohn, K.J. Dy, T.E., Sontheimer, H. With-No-Lysine kinase 3 (WNK3 stimulates glioma invasion by regulating cell volume. *Am J Physiol Cell Physiol* **2011,** *301,* C1150-C1160.
71. Li, L., Xie, D., Yu, S., Ma, M., Fan, K, Chen, J., Xiu, M., Xie, K., Li, Y., Gao, Y. WNK1 interaction with KEAP1 promotes NRF2 stabilization to enhance the oxidative stress response in hepatocellular carcinoma. *Cancer Res* **2024,** *84,* 2776-2791.
72. Kim, S., Kehri, J.H. Inhibition of WNK kinases in NK cells disrupts cellular osmoregulation and control of tumor metastasis. *J Innate Immunol* **2024,** *16,* 451-469.
73. Brandtzaeg, P. Immunobiology of the tonsils and adenoids. *Mucosal Immunol* **2015,** http://dx.doi.org/10.1016/B978-0-12-415847-4.00103-8